PROTEINS: Structure, Function, and Genetics 24:115–133 (1996)

Molecular Dynamics Study of Glucocorticoid Receptor–DNA Binding

Thomas C. Bishop and Klaus Schulten
Beckman Institute, Departments of Chemistry and Physics, University of Illinois at Urbana–Champaign, Urbana, Illinois 61801

ABSTRACT **Molecular dynamics simulations have been conducted to investigate the binding of the glucocorticoid receptor (GR) dimer to DNA. For this purpose simulations of the complex formed by a DNA segment and a dimer of GR–DNA binding domains (GR-DBD) have been carried out, employing an available X-ray structure. A second set of simulations was based on this structure as well, except that the DNA segment was altered to the consensus glucocorticoid response element (GRE). Simulations of a single GR-DBD and of the uncomplexed GRE served as controls. For the simulations, each system was encapsulated in an ellipsoid of water. Protein–DNA interactions, dimer interactions, and DNA structural parameters were analyzed for each system and compared. The consensus GRE is found to yield more favorable and symmetric interactions between the GR-DBDs and the GRE, explaining the ability of the GR dimer to recognize this DNA segment. Further analysis focused on deformations of the DNA that are induced by the binding of GR. The deformations observed involve a 35° bend of the DNA, an unwinding, and a displacement of the helical axis. These deformations are consistent with a mechanism for transcriptional regulation that involves a change of nucleosome packing upon GR binding. Significant protein–protein and protein–DNA interactions, both direct and water mediated, develop due to the deformations of the GRE and are indicative of an increased recognition achieved through DNA deformation. The interactions include direct interactions between the GRE and glycine-458 and serine-459, side groups which differentiate GR from other members of the nuclear hormone receptor family.**

Key words: receptor proteins, estrogen receptor, DNA bending, DNA unwinding, DNA recognition, molecular dynamics

INTRODUCTION

The glucocorticoid receptor (GR) is a member of the family of nuclear hormone receptors that are ligand-inducible transcription activators.[1–3] Nuclear hormone receptors consist of six functional domains, A–F, which are schematically represented for three receptors in Figure 1. The DNA-binding domain (DBD) is a localized domain of the receptor which enables the receptor to bind to a specific DNA sequence as proven by so-called finger swap experiments.[4] This particular domain exhibits a high degree of structure and sequence homology between the various members of the family.[1,3] The amino acid sequence for the rat GR-DBD, a class II zinc-binding motif,[5] is also presented in Figure 1, and is the sequence employed for our study. Twenty-four amino acids appearing in bold letters in Figure 1 are conserved throughout the nuclear hormone receptor family.[6] Upon binding DNA, the reading helix, amino acids 457 through 469, fits into the major groove of the DNA, and the third α-helix, formed by amino acids 492 through 503, is oriented nearly parallel to the DNA axis.

The family of nuclear hormone receptors can be divided into two subfamilies, the estrogen receptor (ER) subfamily and the GR subfamily, according to the DNA sequence that the protein binds and the identity of three key amino acids.[7] The GR subfamily, which also includes the progesterone, androgen, and mineralcorticoid receptors, are identified by the key amino acids Gly-458, Ser-459, and Val-462 as labeled in Figure 1. This subfamily of receptors target the DNA sequence AGAACA, called a half-site. The ER subfamily, which also includes the ecdysteroid, vitamin D_3, thyroid hormone, and retinoic acid receptors, is identified by the key amino acids glutamic acid in place of Gly-458, glycine in place of Ser-459, and alanine or glycine in place of Val-462. The ER subfamily of receptors targets the half-site AGGTCA Thus, these three amino acids and two base pairs are critical in the recognition between the protein and the DNA.[8–10]

Abbreviations: XR, X receptor, where X denotes the receptor name; DBD, DNA binding domain; XRE, X response element, where X denotes the corresponding receptor; rmsd, root mean square deviation; rms, root mean square.

Received April 14, 1995; revision accepted July 7, 1995.
Address reprint requests to Klaus Schulten, Beckman Institute, University of Illinois at Urbana–Champaign, 405 North Matthews, Urbana, IL 61801.

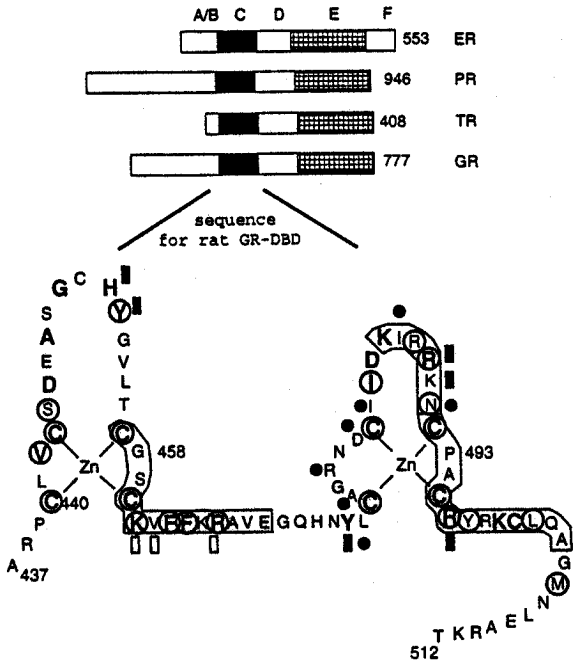

Fig. 1. (Top) A schematic representation of the six functional domains of the estrogen receptor (ER), progesterone receptor (PR), thyroid hormone receptor (TR) and the glucocorticoid receptor (GR). The A/B domains affect transcriptional activity; C is the DNA binding domain, D is the hinge region, and E is the ligand binding domain. (Bottom) The amino acid sequence of the rat GR-DBD used in this study. Circles indicate amino acids which alter transcriptional activity upon site mutagenesis;[56] bold letters indicate conserved amino acids in the nuclear receptor family.[6] Dots denote dimer interactions, solid boxes denote phosphate interactions, and open boxes denote base interactions with the DNA, identified in the crystallographic structure.[24] The amino acids constituting α-helical structures are outlined.

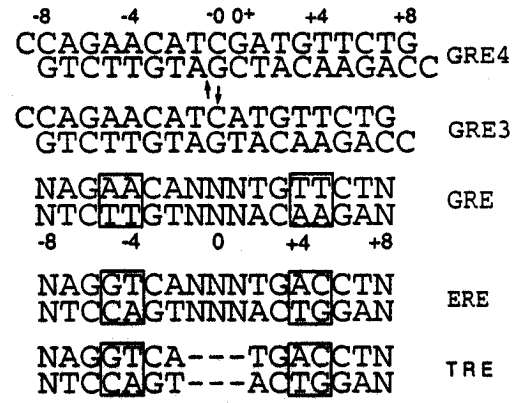

Fig. 2. Consensus sequences for the glucocorticoid response element (GRE), estrogen response element (ERE), and thyroid hormone response element (TRE). N is a variable nucleotide and—is used in this figure for alignment, i.e., for a lack of a nucleotide. Boxes indicate the differences between response element half-sites and arrows indicate the symmetry axes. GRE3 and GRE4 are the specific sequences for the systems pgre3 and pgre4. Numbers indicate the scheme used in this paper for the base pairs.

The sequence of DNA that a receptor targets in vivo is called the response element and will be denoted by GRE (XRE) for the response element of GR. Response elements for three nuclear hormone receptors are shown in Figure 2. A single receptor binds to a half-site, as discussed above; however, the receptors in the nuclear receptor family function primarily as dimers, so that the complete response element consists of two half-sites separated by so-called spacer base pairs. The spacer base pairs are nonspecific, denoted by N in Figure 2, and serve to align the half-sites so that, upon complex formation, the receptors which compose the dimer are oriented for optimal dimer contacts, as well as optimal contacts with the half-sites. A palindromic response element, termed GRE3, constructed from the crystallographic data, is shown along with a consensus GRE in Figure 2. Wild-type ER and GR exist as dimers in solution, and the protein–protein contacts lead to cooperative DNA binding.[11–14] The isolated DBDs of these proteins (see Fig. 1) exist as monomers in solution,[15,16] indicating that not all of the dimer contacts are located in the DBD. The isolated DBDs are, however, capable of recognizing the response element.[12]

Proposed mechanisms for the regulation of transcription by nuclear hormone receptors, although not fully understood, rely on the ability of the protein to affect nucleosome packing. Bending of DNA has been observed for at least 20 different transcription factors; the magnitude of bending varies from 20° to 130°.[17] For ER, the method of gel assay analysis, which determines bending by mobility shifts,[18,19] indicates that the ER-DBD will induce a bend of 34° while the complete receptor, i.e., including domains A–F of Figure 1, produces a bend of 56°.[20,21] These observations of DNA bending for the nuclear hormone receptors along with the observation of response element phasing in nucleosomes[22] suggest that the nuclear hormone receptors weaken the interaction of DNA with histones by altering the conformation of the DNA. However, bending is not observed in the available crystallographic structures of nuclear hormone receptor proteins complexed with DNA. Only minor deviations from B form DNA are observed in the crystallographic structure of the ER-DBD/DNA complex[23] and in the crystallographic structure of the GR-DBD/DNA complex.[24] These negative results might be due to crystal packing, since its effect on the protein–DNA structure is not understood.[17]

Understanding the mechanism of nuclear hormone receptors from the crystal structure of the GR-DBD/DNA complex is further complicated by the fact that the DNA sequence employed is not a natural response element;[24] rather, the central three base pair spacer NNN, as shown in Figure 2, had been replaced by four base pairs NNNN, since the latter yielded crystals that diffracted with higher

resolution. The resulting DNA base pair sequence, labeled GRE4, is also shown in Figure 2.

In the present study we extend our earlier report of GR-induced bending of the GRE.[25] We have employed molecular dynamics simulations to alter the crystal form of the GR-DBD/DNA complex to obtain a GR-DBD dimer complexed with a consensus GRE, i.e., we altered the spacer group NNNN back to the naturally occurring spacer NNN. We studied the resulting system, as well as the NNNN spacer system, under solvent conditions, i.e., without the constraints of a crystal, and have found that without these constraints the GR-DBD significantly alters the conformation of the DNA. In particular, the GR-DBD induces a 35° bend, in agreement with experiments for the ER-DBD,[20,21] and an unwinding of the DNA. The interactions that we report here are primarily due to the deformations of the DNA and are, therefore, not observed in the crystallographic structure which contained near linear B form DNA.[24]

Other simulations based on the same crystallographic structure[26,27] and on a model system[28] have recently been reported. These simulations do not yield the DNA conformational changes that we report here. The simulations by Eriksson et al.[26,27] used the NNNN spacer DNA and, therefore, could not reproduce wild-type protein–DNA interactions. The simulations by Harris et al.[28] employed a 29 base pair sequence of DNA corresponding to the mouse mammory tumor virus GRE, and focused on protein–DNA interactions corresponding to cognate codon/anticodon sequences. Bending and unwinding of the DNA were reported in this study, but were not analyzed quantitatively.

METHODS

Structures

Four systems were investigated by means of molecular dynamics simulations. The system labeled pgre4 contains a near consensus response element (NNNN spacing, GRE4 in Fig. 2) and the GR-DBD dimer; a second system, pgre3, contains a consensus DNA response element (NNN spacing, GRE3 in Fig. 2) and the GR-DBD dimer; a third system, gre, contains only the consensus response element (GRE3); and a forth system, dbd, contains a single DBD of GR. All systems are embedded in an ellipsoidal bath of water as described below. Each of these systems is derived from the crystal structure of the GR-DBD/DNA complex.[24] As stated above, the DNA employed in the crystallographic analysis contained a spacer region, NNNN, of 4 base pairs between half-sites, rather than the naturally occurring NNN. In the crystallographic structure,[24] one monomer, monomer 1, makes contact with a consensus half-site; the other monomer, monomer 2, is displaced by 1 base pair from a consensus half-site, retaining the dimer interactions and forfeiting optimal interaction with DNA.

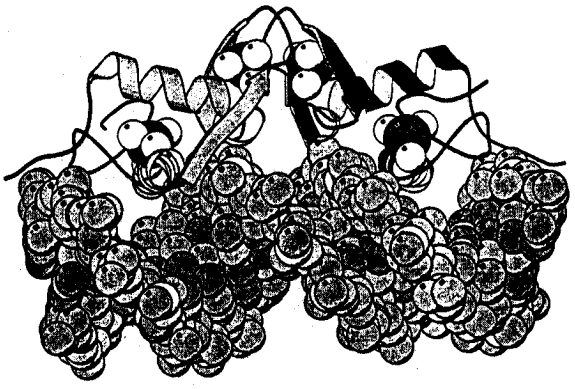

Fig. 3. Ribbons representation of the GR-DBD dimer bound to a consensus GRE. The two reading helices, separated by one helical repeat along the DNA axis, bind in the major groove of each half-site. This configuration requires the minor groove to pass directly beneath the dimer interface. The reading helices are perpendicular to the page and antiparallel to one another. The four zinc ions are represented as van der Waals spheres in the structure.

We employed for the starting structure of the pgre4 system the protein and DNA coordinates reported by Luisi et al.[24] The protein and DNA coordinates for the pgre3 system were obtained from the crystal structure[24] by separating the DNA from the dimer and deleting the +0 base pair in GRE4 (see Fig. 2). Since the DNA is B form, rotating the second segment by 36° and translating it by 3.4 Å along the helical axis properly connected the two segments of DNA. This was accomplished using the coordinate transformation routines available in the structure refinement package X-PLOR.[29] Local defects in the constructed DNA segment were annealed through 500 steps of energy minimization using X-PLOR[29] and allowing only the base pairs adjacent to the site of deletion to relax. The resulting helical parameters of the new DNA strand were those of B form DNA. The DNA was then realigned with the GR-DBD dimer such that the relationship to monomer 1 remained identical to that observed in the crystal structure.[24] This procedure brought monomer 2 into alignment with a consensus DNA half-site while retaining its contact with monomer 1. The resulting complex of the consensus response element, monomer 1, and monomer 2 is presented in Figure 3.

Previous molecular dynamics simulations of DNA have demonstrated that measures must be taken to stabilize the B form helical conformation of DNA. Various methods have been employed including modified charges on the phosphate groups, counterions, water, and/or base pair constraints. Several recent reviews describe the modeling of DNA.[30–33] For our particular protein–DNA system the protein dimer has a positive charge, $+12e$, which partially compensates for the charge of the DNA; however, the resulting net charge of each system is still

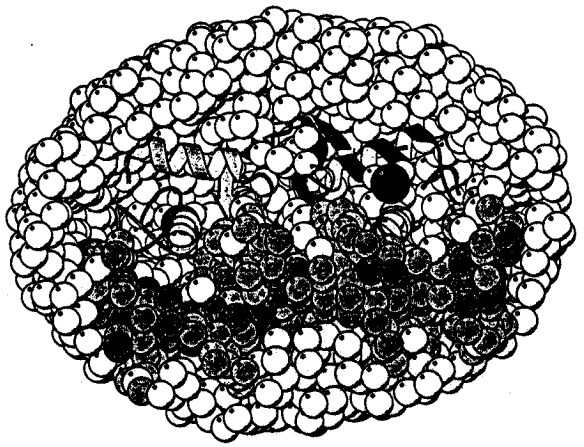

Fig. 4. Cut-away view of the system pgre3 showing the ellipsoid of water surrounding the protein dimer (top of image) and the DNA (bottom of image). The image was generated using MOLSCRIPT.[57]

rather large, namely, $-22e$ for pgre3 and $-24e$ for pgre4.

A short simulation of the GRE3–DBD dimer complex without any water molecules or counterions revealed that the DNA structure was not stable in vacuo and that the DNA rapidly deviated from B form helical parameters unless water was added to the system. Using the algorithm WATER[34] a box of 125 waters, equilibrated to 300 K, was replicated on a grid to encapsulate each system with an ellipsoid of water. The ellipsoidal geometry optimized solvation while minimizing the total number of waters needed to surround the protein–DNA complex. WATER[34] centered the solvent on the system being solvated and searched the space 1.6 Å from each water's oxygen atom; if van der Waals contacts with the protein–DNA system were acceptable, the respective water molecule was included; otherwise, it was not included. No waters were added between the DNA and monomer 1 for either pgre3 or pgre4, except for waters observed in the crystal structure. Waters between monomer 2 and DNA were placed for both the pgre3 and pgre4 systems at positions equivalent to those between DNA and monomer 1. The resulting system, pgre3, is presented in Figure 4.

The system gre was constructed such that the DNA was offset 4 Å along the minor axis from the center of the water capsule; thus, the location of the DNA within the ellipsoid was similar to that of the DNA in pgre3.

Simulations

Information on the molecular dynamics simulations is provided in Table I. Parameters for the all-atom representation of the protein, as well as the DNA segment, were taken from release 3.1 of X-PLOR[29] and were based on CHARMm19 parameters, which included protein–DNA interaction parameters and fully charged phosphates for the nucleic acids. TIP3P parameterization was used for water.[35]

Essentially all simulations were conducted on transputer-based parallel computers using the molecular dynamics program EGO,[36–38] which is compatible with the CHARMm energy routines.[39] EGO does not incorporate cut-off approximations for the nonbonded interactions; instead, full range electrostatic interactions are calculated by means of a distance class algorithm combined with a generalized Verlet integration scheme.[40] The generalized Verlet algorithm satisfies Verlet equivalence and corresponds to an interpolation of forces in a multiple time scale scheme.[41,42]

To avoid the escape of waters during the simulations, a harmonic boundary potential was employed. For this purpose any atom crossing a defined boundary experienced a restoring force linearly proportional to the distance from the boundary and directed normal to the boundary surface. The boundaries were defined as ellipsoids slightly larger than the surfaces of the water baths described above.

The simulations of the systems pgre4, pgre3, gre, and dbd were conducted in *three phases* using a 0.75 fs time step, SHAKE distance constraints[43] for the hydrogen atoms, and the harmonic well restraints for all atoms approaching the surface of the simulated volume. In *phase one* of the simulations 2 ps of energy minimization were conducted. EGO employs a steepest descent minimization technique that removes energy from the system at every time step by rescaling the atomic velocities by a factor of 0.7. The maximum move of any atom for a single integration step was, also, limited to 8×10^{-3} Å.

In the *second phase* of the simulations 2 ps of equilibration dynamics were run and velocities, v, were gradually rescaled according to

$$v_{\text{new}} = v_{\text{old}} \times \sqrt{1 + \left(\frac{T_{\text{target}}}{T} - 1\right) \times \frac{\Delta t}{\tau}} \quad (1)$$

in order to achieve a stable target temperature, T_{target}, of 300 K. Here, T denotes the instantaneous temperature of the system, Δt denotes the integration time step, and τ a coupling constant, chosen as 75 ps.

In the *third phase* of the simulations, molecular dynamics calculations were conducted with Langevin dynamics applied to the waters (γ = 1/ps). This phase of the simulation covered approximately 90 ps for the simulations of pgre4 and pgre3. The systems gre and dbd were each simulated for 45 ps.

Energy Calculations

Protein–DNA and protein–protein nonbonded interaction energies were calculated from the trajectories, at 0.96 ps intervals, using X-PLOR.[29] The atom selections for these calculations included only

TABLE I. Summary of the Methods Used to Conduct Simulations of the Systems pgre3, pgr4, gre, and dbd*

	pgre3	pgre4	gre	dbd
Program	EGO[36,37]			
Processor (nodes)	GCel, T805 (64)		T800 (60)	
Energy function	All atom, modified CHARMM19, TIP3P			
Coulomb evaluation	Full; 8 distance classes[40]			
Integration method	multiple timestop Verlet-II[40]			
Stochastic forces	Applied to all waters			
No. atoms	13,566	13,560	7,475	4,331
No. waters	3,359	3,336	2,112	1,052
Initial coordinates	modified	crystal	modified	crystal
Timestep	0.75 fs	0.75 fs	0.75 fs	0.75 fs
Harmonic well (Å^3)	60 × 60 × 80	60 × 60 × 80	43 × 43 × 86	35 × 40 × 60
Total simulation time	90 ps	90 ps	45 ps	45 ps
% efficiency/node[55]	65	65	72	69
Avg. time/step (s)	24	24	7.8	5.0

*pgre3 consists of water, GR-DBD dimer, and consensus DNA; pgre4 consists of water, GR-DBD dimer, and near-consensus DNA; gre consists of water and consensus DNA; dbd consists of water and a GR-DBD monomer.

atoms of the protein or the DNA; thus, the effects of solvation were not included. The energy functions and parameters used for the analysis with X-PLOR[29] were the same as those employed by EGO, except that a cut-off of 7.5 Å was used in calculations with X-PLOR.[29]

Structure Calculations

The Molecular Dynamics Analysis Toolchest[44,45] was employed for geometric analysis of the trajectories at 1.8 ps intervals. Selected snapshots of the protein and DNA axes produced by this package are presented. The resulting data were also used to calculate the helical repeat,

$$H = \frac{N \times 360^\circ}{\Sigma\tau} \qquad (2)$$

for each trajectory point in order to characterize the overall degree of winding and unwinding of the DNA. $\Sigma\tau$ in (2) denotes the total inter-base pair twist from position −7 to position +7 of a DNA segment, i.e, only the half-sites and the spacer elements are considered. N is equal to the number of base pairs minus one; thus, N is equal to 16 for GRE4, which includes 4 base pairs as the spacer element, and N is equal to 15 for GRE3, which includes 3 base pairs as the spacer element.

The roll, ρ, and tilt, θ, values produced by the Molecular Dynamics Analysis Toolchest[44,45] are measures of inter-base pair angles;[46] nonzero values result in a localized bend, β, of the DNA axis determined by

$$\cos(\beta) = \cos(\theta) \times \cos(\rho) \qquad (3)$$

We evaluated β as a function of sequence position by averaging over the trajectories of pgre3 and pgre4.

The root mean square (rms) fluctuations and root mean square deviations (rmsd) were calculated from the trajectories, at 0.96 ps intervals, using X-PLOR.[29] The rms fluctuations of the protein and DNA backbones were calculated with the average structure as the reference, and the rmsd values of all heavy atoms were calculated with the initial structure as the reference.

Contact Frequency Calculations

In order to characterize the protein–protein and protein–DNA interactions we have calculated so-called contact frequency matrices. To construct these matrices, the trajectories were analyzed with the distance functions in X-PLOR[29] using a 0.96 ps interval between analysis points. For each analysis point an amino acid or base pair was selected, and a search of all atoms located within a radius of 2.5 Å was conducted; the parent amino acids or base pairs were defined as making a contact. The total number of intermolecular contacts between pairs of residues was then determined and presented in the form of contact matrices. Our use of the term "contact," therefore, identifies hydrogen bonds, salt bridges, or van der Waals contacts.

Hydrogen Bond and Water Bridge Calculations

To differentiate the nature of the contacts evaluated above, we have analyzed the intermolecular hydrogen bonds. We have also determined which waters form intermolecular bridges through hydrogen bonding interactions. The hydrogen bonds were evaluated with X-PLOR[29] at 96 fs intervals. A hydrogen bond is defined by an acceptor–hydrogen–donor angle of less than 60° from linear and an acceptor donor distance of less than 3.5 Å. A percent occupancy for each hydrogen bond was determined as the number of occurrences of a particular hydro-

gen bond divided by the number of analysis points. A similar analysis was carried out to investigate the waters which form bridges between the protein and the DNA and between the protein monomers. For our analysis, a water bridge occurs between any molecules that hydrogen bond to a common water molecule; bridges which involve multiple waters are counted only once per trajectory point.

Notation

Protein elements of the simulated structures will be identified below using a notation introduced best by way of an example. We denote by P3-2-Lys-486-NH_3 an element of the protein P3-2, namely the NH_3 moiety of its Lys-486 residue. P3-2 designates monomer 2 of pgre3; other notations used in this place are P4-1, P4-2, and P3-1 for monomer 1 of pgre4, etc. The protein and residue, e.g., P3-2 and Lys-486, are used individually or combined; thus, Asn-491 refers to asparagines at position 491 in any of the systems, and P3-1,2 refers to monomer 1 or 2 of pgre3. DNA components of the structures are identified as GRE3-T−2, where GRE3 designates the DNA segment in pgre3 and T−2 denotes the deoxythymidylate residue at position −2. The DNA segments in pgre4 and gre are denoted GRE4 and GRE, respectively. C±3 refers to deoxycytidylates at position three and minus three in any of the systems. A positive position for nucleotides, e.g., C+3, will indicate a nucleotide of the half-site in contact with monomer 2 and a negative position, e.g., C−3, will indicate a nucleotide of the half-site in contact with monomer 1, i.e., the monomer that initially exhibits more favorable interactions with the DNA.

ENERGETIC ANALYSIS

Protein–DNA and protein–protein interaction energies are used as an indication of the degree of recognition and dimerization between the protein and DNA and between the protein monomers over the course of our simulations.

Protein–DNA Interactions

The protein–DNA interaction energies, shown in Figure 5, demonstrate that the proteins in pgre3 associate more strongly with the DNA than the proteins in pgre4, reflecting the fact that pgre3 contains the proper DNA target for GR and that it is "recognized" by the protein. The protein–DNA interaction stabilizes over a time course of 40 ps for pgre3; after this, the interaction energy remains approximately constant for the remainder of the simulation. For pgre4, the protein–DNA interaction stabilizes within 7 ps, the faster equilibration time being due to the fact that pgre4 represents the crystal structure, which, presumably, is equilibrated. After the systems have stabilized in the respective simulations, an energy difference of more than 200 kcal/mol between the protein–DNA complex of pgre3 and that of pgre4 indicates the dimers ability to discriminate between the two DNA sequences. For both, pgre3 and pgre4, the protein–DNA interaction energy is nearly evenly divided among the two monomers. Comparing the monomers to one another within each simulation, one observes that P4-1, i.e., the monomer optimally associated with DNA in the initial structure, maintains a consistently stronger interaction with the DNA than P4-2. The same is true when P3-1 and P3-2 are compared. This result suggests that the simulations, most likely, have not yet achieved a completely equilibrated state which would be characterized by a symmetric association of the two monomers.

Protein–Protein Interactions

The protein–protein interaction energies, presented in Figure 6, differ for pgre3 and pgre4. The interaction energies between P4-2 and P4-1 reflect a gradual destabilization of the dimer, arriving at a constant value of −150 kcal/mol after 25 ps. The altered DNA sequence in pgre3 allows a better fit of the two protein surfaces involved in the dimer contact as reflected in a decrease of the P3-2 to P3-1 interaction energy during the first 40 ps, the energy reaching a value of −230 kcal/mol. The interaction energy increases to −175 kcal/mol at 50 ps, but still remains more favorable than in the case of pgre4. These interaction energies do not include the effects of solvation, so that water bridges partially compensate for this loss of interaction in pgre3. The synchronous stabilization of protein–protein and protein–DNA interactions implies a cooperative character of the binding of the GR-DBD dimer to DNA. In this respect, it should be noted that the decrease of the total protein–DNA interaction energy for pgre3 measures over 300 kcal/mol, a value which is significantly larger than the sum of the separate protein–protein interaction energies for P3-1 and P3-2, indicating that the protein–DNA interactions are dominant. Figure 6 demonstrates that the primary contribution to the protein–protein interaction stems from electrostatics; the salt bridges between Arg-479 and Asp-481 are the main contributors for each simulation, as discussed below.

MOLECULAR CONFORMATION

Snapshots of the protein and DNA backbone axes, shown in Figure 7, illustrate the conformational changes observed over the course of the simulations of pgre4 and pgre3. A bending of the DNA axis over the course of the simulations can clearly be discerned. In Figure 7A, which shows the conformation at the end of *phase 2* of our simulations, the DNA is nearly linear as in the original crystallographic structure. In Figure 7B, showing the structures after approximately 22 ps of simulation in *phase 3*, the DNA segments of both pgre4 and pgre3 have been distorted to form a localized bend near the spacer

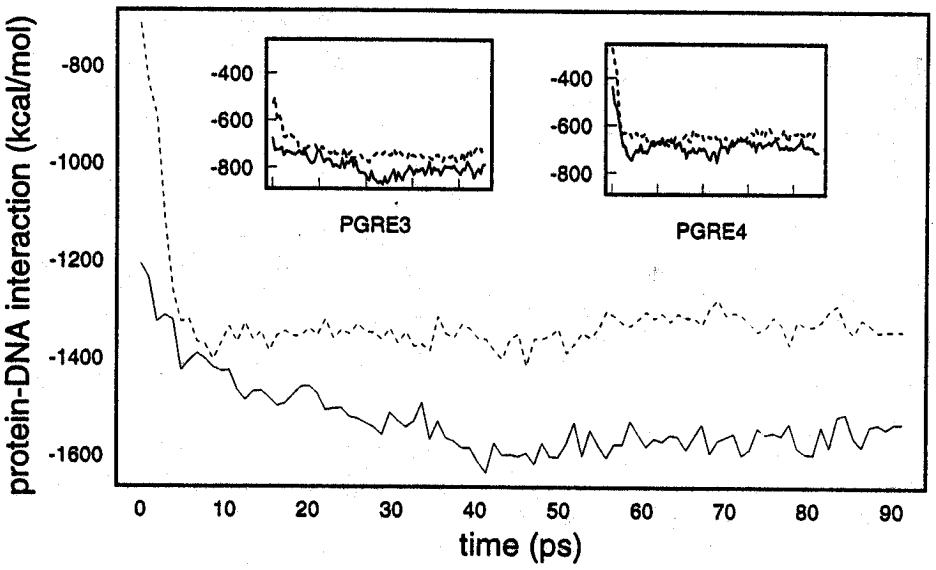

Fig. 5. Total nonbonded protein–DNA interaction energy as a function of time; pgre3 (solid line), pgre4 (dotted line). Insets indicate contributions of the individual monomers P4-1 (solid line, right inset), P3-1 (solid line, left inset), P4-2 (dotted line, right inset), and P3-2 (dotted line, left inset).

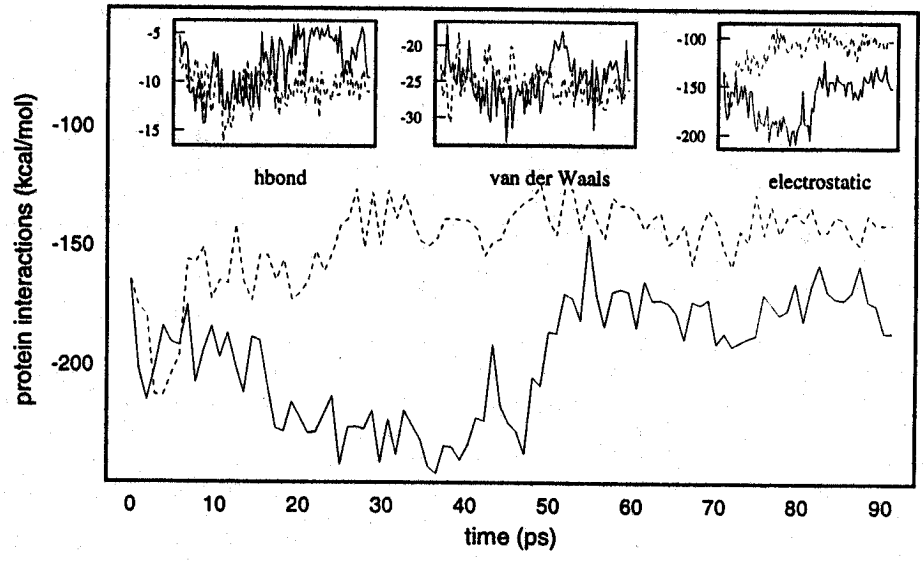

Fig. 6. Total nonbonded protein–protein interaction energy as a function of time; pgre3 (solid line), pgre4 (dotted line). Inserts indicate contributions from explicit hydrogen bonding, van der Waals, and electrostatics energy functions.

groups NNNN and NNN, respectively. The ends of the DNA segment have developed further deviations from linear B form DNA at 44 ps, most obvious for the case of GRE4, as shown in Figure 7C. These distortions are due to hydrogen bonds involving Cys-450, His-451, and Lys-511 and the phosphate groups of GRE4 + 7,8. The interactions exist for each monomer in both pgre3 and pgre4. The DNA segments in pgre3 and pgre4 remain bent throughout the latter parts of *phase 3* of our simulations.

During the simulations, P3-2, appearing on the left side of each frame, establishes closer contact to the DNA than P4-2. This is discernible as a downward translation of P3-2 relative to P4-2 in Figure 7C and D. P4-1 or P3-1 do not show such a translation, as evidenced by the overlap of the respective protein folds in Figure 7. This behavior indicates that the interaction of monomer 1 with the DNA is optimal in the initial structure, i.e., the crystal structure. The translation of P3-2 is further sup-

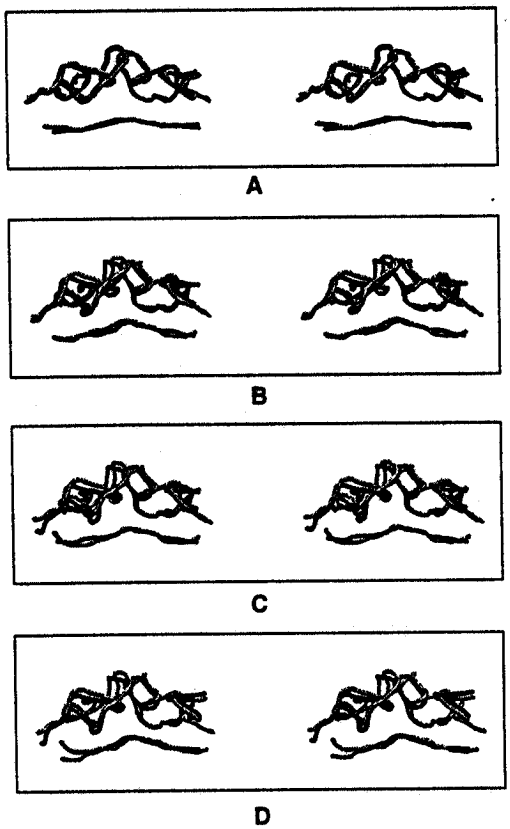

Fig. 7. Molecular axes determined using the Molecular Dynamics Analysis Toolchest[44,45] and displayed as stereo images with the visualization package vmd.[54] A, B, C, and D correspond to snapshots taken at t = 2, 22, 44, and 66 ps. pgre3 (black); pgre4 (gray). Monomer 2 appears on the left and monomer 1 appears on the right side of each frame.

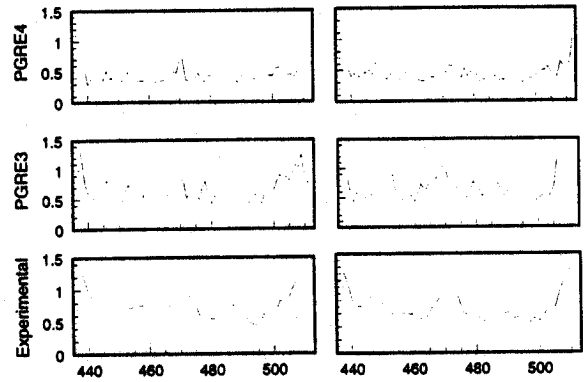

Fig. 8. Protein rms fluctuations based on the last 45 ps of the simulations (labeled pgre3 and pgre4) averaged over the peptide backbone of each amino acid. Data for monomer 1 on the left, data for monomer 2 on the right. Data determined from the crystallographic temperature factors are denoted "Experimental."

ported by P3-2's rmsd from the initial structure. P3-2 develops a larger rmsd than any of the protein elements, P3-1, P4-1, P4-2, or dbd. The motion of P3-2 toward the DNA affects the protein–DNA interactions, as well as the relative orientation of P3-1 to P3-2, and, hence, the dimer interactions. The interaction energies presented in Figures 5 and 6, and discussed above, are indicative of the respective behavior.

Protein Fluctuations

Root mean square fluctuation values for the backbone atoms of each monomer are presented in Figure 8. Elevated rms fluctuation values peak at Gly-470 and are elevated throughout the reading helix, amino acids 457 through 469. The rms fluctuation values decrease with increasing distance from Gly-470, but the Φ and Ψ angles in this region demonstrate relatively small fluctuations about ideal α-helical values. Since rms fluctuation values reflect motions in a fixed reference frame, while the Φ and Ψ angles describe motions in a relative reference frame, our simulations indicate that the reading helix fluctuates as an integrated structural element. This is not true for the protein segments immediately following the reading helices, namely amino acids Gln-471 through Tyr-474, which are located on the carboxy side of Gly-470. These amino acids show significant rms fluctuation values, as well as significant differences in Φ and Ψ angles between proteins P3-1, P3-2, P4-1, and P4-2. For P3-1 and P4-1, amino acids His-472, Asn-473, and Tyr-474 are making strong contacts to the DNA and exhibit lower rms fluctuation values compared to the values observed for P3-2 and P4-2. For P3-2 and P4-2, the side chains are oriented away from the DNA and, therefore, contact the solvent. The result is a difference in profiles of the rms fluctuation values for monomer 1 and monomer 2 in this region of the protein.

We conclude that the reading helix, amino acids 457–469, fluctuates as a single structural element and that the dynamics and conformation of amino acids Gln-471 to Asn-474 depend on local interactions and conformation. The implication is that dimerization and DNA contacts of amino acids not located in the reading helix can influence the dynamics of the reading helix. Our conclusion is supported by observations of binding cooperativity,[11,14,47] and by a simulation of the GR-DBD/GRE4 complex based on the same crytallographic structure.[27]

DNA Twist

The helical repeat, H, is a measure of the winding and unwinding of the DNA, and has an initial value of 10 bp/turn for pgre4, as in the crystal structure.[24] pgre3 and gre, which were constructed from pgre4, also have initial values of 10 bp/turn. H increases, at different rates, over the course of each simulation, as demonstrated in Figure 9, indicating an unwinding of the DNA segments. We suggest that the un-

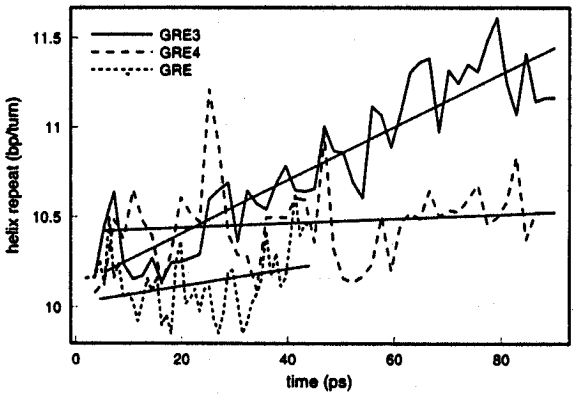

Fig. 9. Helical repeat for each response element calculated from the twist values: simulation gre (line ending at 45 ps), pgre3 (solid line), pgre4 (dotted line). The lines, least-square-fit to the data, have positive slope which indicates unwinding of the DNA. pgre3 has the greatest slope, therefore undergoing the greatest degree of unwinding.

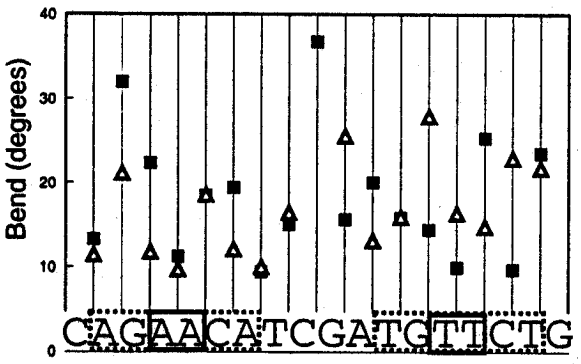

Fig. 10. Local bend angles, averaged over the simulations pgre3 (triangles) and pgre4 (squares). Solid boxes indicate base pairs that distinquish an ERE from a GRE (see Fig. 2), dotted boxes indicate half-sites. There is no measure of the bend angle for the central C-G base pair step for the simulation of pgre3; this corresponds to the site of deletion of a base pair from pgre4 in order to construct pgre3.

winding of GRE4 and GRE represents a relaxation of DNA from 10.0 bp/turn in the crystal environment toward 10.3–10.6 bp/turn expected for a solution environment,[46,48,49] while the larger slope of H for GRE3 indicates that unwinding of the proper target site is further driven by interactions with the protein. Figure 9 indicates an average value of 10.2 bp/turn near 40 ps for GRE, an average value of 10.5 bp/turn near 80 ps for GRE4, and an average value of 11.2 bp/turn near 80 ps for GRE3. The total twist has not achieved a stationary value over the course of our simulations; therefore, we emphasize the difference in the slopes of H rather than the specific values of the twist.

DNA Bending

All inter-base pair positions exhibit some degree of bend as indicated by Figure 10, thus contributing to a writhed conformation of the helical axis. In both systems, pgre3 and pgre4, the writhe is manifest as a bend away from the protein (Fig. 11, bottom) and as a displacement of the helical axis in a plane perpendicular to this bend (Fig. 11, top).

The bend away from the protein is located in the spacer region NNN or NNNN and results from larger values of roll observed for NNN and NNNN. In the case of pgre4, the major contribution to this bend arises between GRE4−0 and GRE4+0, while in the case of pgre3 the bend arises mainly from positions GRE3−1 to GRE3−0 and GRE3−0 to GRE3+1. To characterize the overall bend of the DNA, the angle between the axis of each DNA half-site has been measured. A bend of 35° can be discerned in Figure 11.

The displacement of the helical axis results from two other bends that lie in a plane perpendicular to the plane of the first bend and are directed so as to cancel each other. This is a property dictated by the

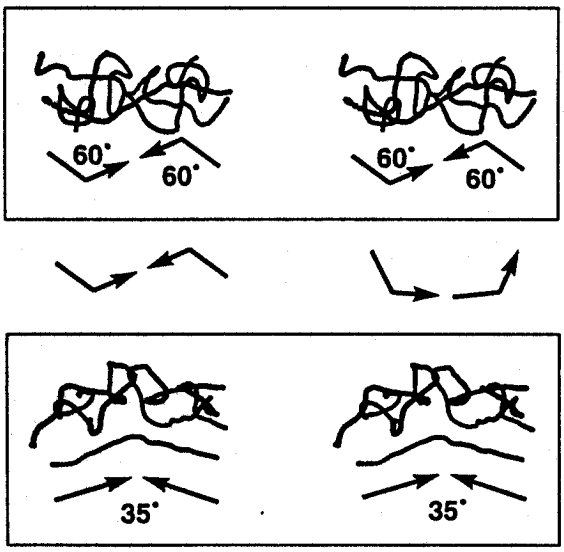

Fig. 11. Stereo representations of the pgre3 complex after 70 ps of molecular dynamics simulation. View with the DNA located in front of the protein (top), and with the DNA below the protein (bottom). Angles indicate deviation from linearity, and arrows indicate the direction of the half-site sequences. Altering the protein–half-site symmetry affects conformation in the plane corresponding to the top view (middle), but will not affect conformation in the plane corresponding to the bottom view.

symmetry of the DNA half-sites and the corresponding symmetry of the monomers, as demonstrated in Figure 11. If the half-sites and monomers where arranged as direct repeats, i.e., head-to-tail rather than head-to-head, these bends would be additive. In other words, if the protein bends the DNA "to the left" then direct repeats of the half-sites will have two left bends, while an inverted repeat of the half-sites will have a "left" bend coupled with a "right" bend. These arguments apply, for the present system, only to bends that lie in a plane which is par-

allel to the plane that intersects the two reading helices. The displacement results from local bends which are located between positions +3 to +4, −4 to −3, +6 to +7, and −7 to −6, as is discernible in Figure 10. Average roll values for pgre3 are 27° for +3 to +4, 16° for −3 to −4, 20° for +6 to +7, and 17° for −6 to −7. The reader may note that positions ±3 and ±4 also differ in base pair composition for GRE and ERE (see Fig. 2) such that GRE and ERE may exhibit different bends when associated with the respective receptors.

Such deviations from linear B form DNA have not been observed to this degree in other simulations[27,28] or in crystallographic structures of related systems.[23,24] The greater deviations from linearity that we observe result in additional protein–DNA and protein–protein interactions, as discussed below.

PROTEIN–DNA INTERACTIONS

Protein–DNA contacts, presented in Figure 12, and water bridges, presented in Tables II and III, indicate significant interactions during our simulations that were not reported in the crystallographic analysis.[24] These interactions include direct interactions with DNA involving Gly-458, Ser-459, Phe-463, Lys-465, Lys-486, Lys-490, and Pro-493 and water bridges involving Ser-459, Phe-463, and Glu-469. Some of the direct interactions are within the limits of the resolution and fluctuations obtained for monomer 1 in the crystallographic structure. The direct interactions are indicative of the greater degree of recognition achieved in our simulations as the DNA deviates from a linear B form conformation and are the primary focus of our analysis of protein–DNA interactions. His-472, Asp-473, and Tyr-474 will also be discussed since these amino acids violate the symmetric nature of the system. We observe interactions between the reading helix and DNA involving Lys-461, Val-462, and Arg-466. Although these interactions are significant, they will not be discussed in detail since these interactions were similar to those reported in the crystallographic analysis.[24]

Alignment and Distribution

The protein–DNA contact matrices for pgre4 and pgre3, presented in Figure 12, show that the contacts between DNA and P3-2 are shifted by 1 base pair relative to those of P4-2. This result, combined with the protein–DNA interaction energies, proves that removal of the additional spacer base pair from pgre4 was effective in realigning P3-2 with its recognition half-site. The majority of the protein–DNA contacts observed in the simulations occur with amino acids that belong to the α-helical segments of the monomers, indicated by the shaded regions in Figure 12.

The reading helices, amino acids 457–469, are able to make DNA contacts that span each half-site. In pgre3, neither reading helix makes contact with the spacer region NNN while the added spacer base pair in pgre4 offsets alignment of the reading helix such that the reading helix of P4-2 contacts NNNN. The contact data indicate that the reading helices of pgre3 have approximately 33% more contact with the DNA than the corresponding reading helices in pgre4. The distribution of these contacts is relatively similar for pgre4 and pgre3, with the exception of the shift noted above.

Glycine-458 and Serine-459

Gly-458 obtains an average interaction energy with DNA of approximately −5 kcal/mol for P3-2, P3-1, and P4-2 and −10 kcal/mol for P4-1. For pgre3 the interactions are van der Waals contacts between the α-hydrogen of each Gly-458 and GRE3-T±5-CH_3. P4-1 exhibits a similar interaction, but P4-2, as previously noted, is out of register by 1 base pair.

The Ser-459s of P3-1, P3-2, and P4-1 each achieves average interactions with DNA of approximately −35 kcal/mol, while P4-2-Ser-459 achieves only an interaction with DNA of −20 kcal/mol. In pgre3, these interactions are van der Waals contacts between the backbone atoms of the Ser-459s and the respective GRE3-T±4-CH_3 groups, while the Ser-459-OHs hydrogen bond to the respective GRE3-T±4-OP_4 groups, as listed in Table IV. The interactions are similar for P4-1, but the corresponding hydrogen bond is replaced by a water bridge for P4-2-Ser-459-OH, as listed in Tables III and V. Water bridges provide further stability for the interactions involving Ser-459 as shown in Tables II and III.

The direct contacts that Gly-458 and Ser-459 achieve with the DNA indicate that the reading helix has descended further into the major groove, corresponding to its greater recognition. Concomitant van der Waals contacts develop between P3-1,2-Val-462-CH_3 and GRE3-T±5-CH_3. Our results help explain the role of these three amino acids in differentiating an ER-type from a GR-type receptor, which was not established unambiguously in the crystallographic structure.[24] The interactions discussed above are illustrated in Figure 13a.

Phenylalanine-463 and Proline-493

The side chains of Phe-463, a conserved amino acid in the nuclear receptor family, and of Pro-493 form a hydrophobic region of each monomer which contacts elements of the phosphodiester linkage, namely GRE-T±2-H3′, H5′, and H5″. This fixes the amino acids between the phosphates GRE-T±2 and GRE-G±3. A water bridge exists between P3-1-Phe-463-O and GRE3-T-2-OP_4, i.e., the adjacent phosphate, as listed in Table II. The Phe-463–Pro-493 region of each monomer borders the dimer interface, and achieves van der Waals contact only after the DNA bends into the dimer region, achieving approx-

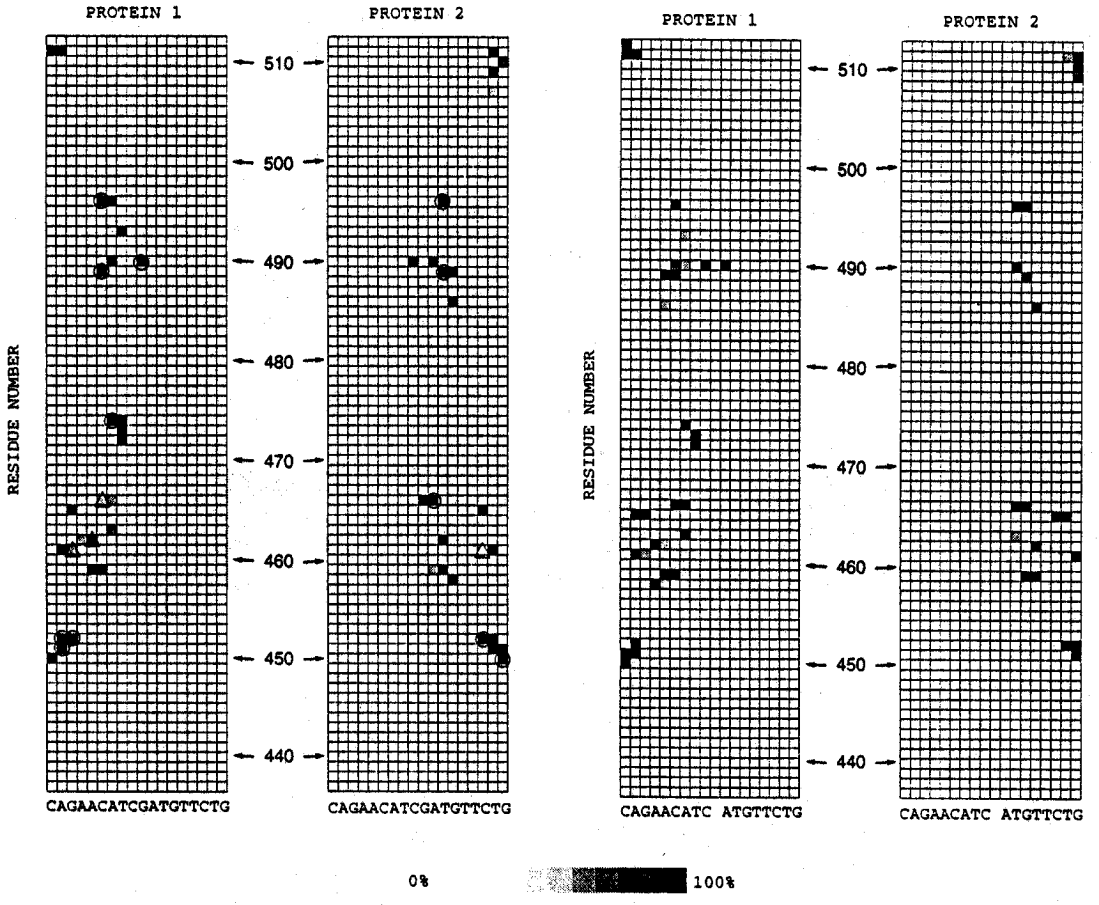

Fig. 12. Contact matrices for each monomer of pgre4 (left side; P4-1, P4-2), pgre3 (right side; P3-1, P3-2). Gray scale indicates frequency of contact between the amino acids (rows) and nucleotide pairs (columns). Circles indicate phosphate contacts; triangles indicate DNA base contacts as reported in the crystallographic analysis.[24] α-Helical segments are shaded.

imately −15 kcal/mol of interaction energy for each hydrophobic region. These contacts are a direct result of DNA bending and are further evidence of the tighter association of the protein with the DNA described above. The contacts are displayed in Figure 13b and have not been previously reported.

Lysine-465

The contacts between Lys-465, which is located in the reading helix, and G±6 or A±7 involve salt bridges and a hydrogen bond, listed in Tables IV and V. A water bridge between P4-2-lys465 and GRE4-G+6-O3′ is also observed (Table III). Our simulations indicate that each Lys-465 achieves an interaction energy with DNA of approximately −90 kcal/mol, while P3-2-Lys-465 undergoes a transition in less than 20 ps to achieve a total interaction of approximately −120 kcal/mol. P3-2-Lys-465-NH_3 bridges the phosphates of GRE3+G6 and GRE3+A7, while P4-1,2-Lys-465 and P3-1-Lys-465 form salt bridges only with the respective G±6-OP_4. Figure 13c displays the contacts for P3-2-Lys-465. The interactions between charged amino acids and phosphate groups of the nucleic acid may be overemphasized in our simulations due to a lack of counterions.

Histidine-472, Asparagine-473, and Tyrosine-474

Amino acids His-472, Asn-473, and Tyr-474 violate the relative symmetry of the protein–DNA contacts, as is evidenced by Figure 12. This asymmetry was reported in the crystallographic analysis.[24] P4,3-1-Asn-473 and P4,3-1-Tyr-474 hydrogen bond with the phosphate groups at A−1 and T−2, as listed in Tables V and IV, while neither of these contacts are observed for P4-2 or P3-2. We also observe asymmetric water bridges between P3-1-Tyr-474 and GRE3-T−2-OP_4 as listed in Table II, and between P4-1-Asn-473 and GRE4-G−0-O3′ and between P4-1-Asn-473 and GRE4-A−1-O4′, as shown in Table III. For P4-2 and P3-2 the side chains of His-472, Asp-473, and Tyr-474 are directed away from the complex and contact only solvent molecules. These interactions are not sequence specific and may serve to increase the nonspecific affinity of

TABLE II. Water Bridges Contributing to Protein–DNA Interactions for pgre3

	DNA	Occupancy (%)
Monomer 1		
His-451 NE2-HE2	C−8 O2P	57.6
Ser-459 N-HN	T−4 O5′	33.4
Phe-463 O	T−2 O2P	47.1
Arg-466 NE-HE	A−1 O3′	45.7
Arg-466 NH2-HH22	T−2 O4′	48.1
Arg-466 NH2-HH22	T−2 O5′	61.6
Tyr-474 OH	T−2 O2P	34.2
Lys-486 O	G−3 O1P	63.3
Ile-487 O	A+1 O2P	46.2
Lys-490 NZ-HZ3	T−2 O3′	39.4
Lys-490 NZ-HZ3	G−3 O4′	61.6
Leu-507 O	G−6 O2P	36.0
Arg-510 O	A−7 O1P	80.4
Lys-511 NZ-HZ3	G−6 O1P	52.8
Thr-512 OT1	C−9 O3′	44.1
Thr-512 OT1	C−8 O1P	47.3
Monomer 2		
Tyr-452 OH	G+6 N7	40.1
Ser-459 N-HN	T+4 O2P	54.0
Ser-459 N-HN	T+5 O2P	39.3
Ser-459 OG	T+4 O2P	50.1
Arg-466 NH2-HH22	T+2 O2P	73.3
Arg-466 NH2-HH22	T+2 O5′	65.6
Glu-469 OE2	G+6 O1P	33.3
Glu-469 OE2	G+6 O2P	57.4
Glu-469 OE2	G+6 O4′	49.5
Glu-469 OE2	G+6 O5′	59.1
Arg-489 O	T+2 O1P	43.3
Lys-490 NZ-HZ1	A+1 O4′	49.1
Lys-490 NZ-HZ1	T+2 O4′	48.8
Lys-490 NZ-HZ3	G−0 N3	58.1
Lys-490 NZ-HZ3	A−1 O4′	56.2
Lys-490 NZ-HZ3	G−0 N2 −H21	36.9
Asn-491 N-HN	T+2 O1P	37.2
Arg-510 NH1-HH12	C+8 O1P	53.2
Arg-511 NZ-HZ1	C+8 O2	35.6

TABLE III. Water Bridges Contributing to Protein–DNA Interactions for pgre4

	DNA	Occupancy (%)
Monomer 1		
Lys-461 NZ-HZ1	T−5 O4	47.6
Arg-466 NH1-HH12	A−1 O5′	39.5
Arg-466 NH1-HH12	T−2 O2P	38.9
Asn-473 ND2-HD22	G−0 O3′	50.6
Asn-473 ND2-HD22	A−1 O4′	40.6
Arg-489 NH1-HH12	G−3 O1P	77.2
Lys-490 O	A−1 O3′	37.3
Leu-507 O	G−6 O1P	55.0
Ala-509 N-HN	G−6 O1P	52.7
Lys-511 NZ-HZ3	A−7 O3′	45.6
Monomer 2		
Ser-459 OG-HG1	G+3 O2P	44.7
Ser-459 N-HN	G+3 O2P	71.8
Lys-461 NZ-HZ2	G+6 N7	63.1
Lys-461 NZ-HZ2	G+6 O6	38.0
Lys-461 NZ-HZ2	A+5 N6 −H61	45.3
Lys-465 NZ-HZ2	G+6 O3′	42.2
Glu-469 OE1	A+5 O1P	40.0
Lys-486 O	T+2 O1P	70.2
Arg-489 N-HN	T+2 O1P	69.6
Lys-490 NZ-HZ1	A+1 O3′	33.3
Lys-490 NZ-HZ1	A+1 O4′	38.5
Arg-496 NH2-HH22	A+1 O2P	34.7
Arg-496 NH2-HH22	A+1 O5′	35.8
Leu-507 O	G+6 O1P	37.4
Ala-509 O	C+8 O3′	67.9
Arg-510 NE-HE	C+9 O3′	35.5
Arg-510 NE-HE	C+8 O1P	49.1

the protein for DNA as the protein diffuses along the DNA in search of its response element. As demonstrated above, these amino acids influence the orientation and dynamics of the reading helix.

Lysine-486

Tables IV and V indicate that the P3-1,2-Lys-486-NH_3 and P4-2-Lys-486-NH_3 groups form salt bridges with the corresponding T±4-OP_4 groups, achieving an interaction energy of approximately −60 kcal/mol each. For P3-1-Lys-486, the salt bridge is formed around 38 ps; the corresponding bond does not form for P4-1. Water bridges augment these interactions for P3-1 (see Table II) and P4-2 (see Table III).

Lys-486 is at the amino end of the second α-helix, which is formed by amino acids 486 through 491; the side chains of P3-2-Lys-486 and P3-1-Lys-486 are oriented so as to form an extension along this helical axis. At the carboxy end of this α-helix is Asn-491, and the symmetry of the dimer allows P3-1-Asn-491 to make a stable contact to P3-2-Asn-491. This arrangement connects the two α-helical segments into one unit, while the side chains of the Lys-486s extend in opposite directions and draw the DNA into closer contact with the protein. These protein–protein and protein–DNA interactions, which are located at both ends of the second α-helix and exist only upon complex formation, certainly affect the stability of this region.

Lysine-490

The length of the side chain of Lys-490 allows it to make contacts that span up to 5 base pairs, as can be seen in Figure 12. Lys-490 is the only amino acid which makes contacts in the minor groove of the spacer region. In the case of P3-1-Lys-490, the side chain is almost fully extended into the minor groove of GRE3, making contacts with both strands of DNA in the spacer region, NNN, hydrogen bonding to GRE3-G0-O4′ (Table IV) and achieving an interaction energy of approximately −80 kcal/mol. Water bridges to GRE3-T−2 and GRE3-G−3 extend the

TABLE IV. Hydrogen Bonds Contributing to Protein–DNA Interactions for pgre3

	DNA	Occupancy (%)
Monomer 1		
Cys-450 N-HN	C−8 O1P	100
His-451 ND1-HD1	C−8 O3′	90
Tyr-452 N-HN	A−7 O1P	100
Tyr-452 OH-HH	A−7 O5′	83
Ser-459 OG-HG1	T−4 O2P	100
Lys-461 NZ-HZ2	A−7 N7	56
Lys-461 NZ-HZ2	G−6 N7	68
Lys-461 NZ-HZ3	A−7 O2P	100
Lys-465 NZ-HZ3	G−6 O2P	100
Arg-466 NH1-HH12	G−3 O6	71
Arg-466 NH2-HH21	G−3 N7	56
Arg-466 NH2-HH21	G−3 O6	56
Asn-473 N-HN	A−1 O1P	100
Tyr-474 OH-HH	T−2 O2P	100
Lys-486 NZ-HZ2	T−4 O1P	60
Arg-489 NE-HE	G−3 O1P	100
Arg-489 NH1-HH11	G−3 O1P	51
Arg-489 NH1-HH11	G−3 O5′	93
Arg-489 NH1-HH12	T−4 O2P	100
Lys-490 NZ-HZ2	C−0 O4′	95
Arg-496 NH1-HH11	G−3 O2P	36
Arg-496 NH2-HH22	G−3 O2P	99
Lys-511 NZ-HZ2	A−7 O3′	81
Tyr-512 N-HN	C−8 O4′	97
Monomer 2		
Tyr-452 N-HN	C+8 O1P	100
Tyr-452 OH-HH	A+7 O2P	100
Ser-459 OG-HG1	T+4 O2P	100
Lys-461 NZ-HZ3	C+8 O2P	96
Lys-465 NZ-HZ2	G+6 O2P	88
Lys-465 NZ-HZ3	A+7 O1P	100
Arg-466 NH1-HH12	G+3 O2P	82
Arg-466 NH2-HH21	G+3 O2P	96
Lys-486 NZ-HZ3	T+4 O1P	96
Arg-489 NE-HE	G+3 O1P	100
Arg-496 NH1-HH11	G+3 O1P	100
Arg-496 NH2-HH21	T+2 O1P	99
Arg-496 NH2-HH22	T+2 O3′	100
Tyr-511 NZ-HZ2	C+8 O3′	100

TABLE V. Hydrogen Bonds Contributing to Protein–DNA Interactions for pgre4

	DNA	Occupancy (%)
Monomer 1		
Cys-450 N-HN	C−8 O1P	100
His-451 ND1-HD1	A−7 O2P	100
Tyr-452 N-HN	A−7 O1P	100
Tyr-452 OH-HH	G−6 O2P	100
Ser-459 N-HN	T−4 O2P	88
Ser-459 OG-HG1	T−4 O2P	67
Lys-461 NZ-HZ2	G−6 N7	37
Lys-465 NZ-HZ1	G−6 O2P	94
Lys-465 NZ-HZ3	G−6 O5′	89
Asn-473 N-HN	A−1 O1P	97
Tyr-474 OH-HH	T−2 O2P	100
Arg-489 NE-HE	G−3 O1P	100
Lys-490 NZ-HZ1	G+0 O1P	94
Arg-496 NH1-HH11	G−3 O2P	80
Arg-496 NH2-HH21	G−3 O2P	96
Arg-496 NH2-HH22	T−2 O1P	96
Lys-511 NZ-HZ2	A−7 O4′	100
Monomer 2		
Cys-450 N-HN	C+8 O1P	100
Tyr-452 N-HN	A+7 O1P	100
Tyr-452 OH-HH	G+6 O2P	98
Lys-465 NZ-HZ3	G+6 O1P	97
Arg-466 NH2-HH22	A+1 O1P	98
Lys-486 NZ-HZ2	G+3 O1P	97
Arg-489 NE-HE	T+2 O1P	46
Arg-489 NE-HE	T+2 O2P	47
Arg-489 NH1-HH11	G+3 O2P	97
Arg-489 NH1-HH12	T+2 O5′	97
Lys-490 NZ-HZ2	G−0 N3	87
Lys-490 NZ-HZ3	G−0 O4′	88
Arg-496 NH1-HH11	T+2 O2P	55
Arg-496 NH2-HH21	T+2 O2P	100
Lys-511 NZ-HZ1	A+7 O4′	93

indirect contacts of P3-1-Lys-490 to also include the half-site, as listed in Table II. As shown in Figure 12, P3-2-Lys-490 does not form as extensive a set of contacts with the DNA as P3-1-Lys-490 does, resulting in a difference in interaction energy of approximately 50 kcal/mol. However, P3-2-Lys-490 compensates for this with a more extensive water bridging network in the minor groove that spans the length of the spacer region, NNN, as indicated in Table II. Both of the Lys-490s in pgre4 are extended into the minor groove of the spacer region, NNNN, and each crosses the axis of symmetry of GRE4 to contact GRE4-G±0 as listed in Table V. Each of P4-1,2-Lys-490 achieves an interaction with the DNA of approximately −80 kcal/mol, indicating their similarity in conformation to P3-1-Lys-490 (see Fig. 12).

We conclude that the extension of Lys-490 and the associated water bridges into the minor groove of the spacer region serves as a wedge that facilitates the bending of the DNA as it is drawn into closer contact with the protein. The violation of symmetry for pgre3 may be due to residual effects from the construction of pgre3 that have locked P3-2-Lys-490 into a particular conformation.

Protein–DNA Water Bridges

In addition to water bridges, which, as described, augment the direct protein–DNA contacts, several other water bridges, listed in Tables II and III, link the protein to the DNA with indirect contacts. The most significant water bridge involves P4,3-2-Glu-469, the carboxy terminus of the reading helix, and GRE-G+6. This water bridge may be of assistance in aligning the reading helix in the major groove as recognition develops. The lack of P4,3-1-Glu-469 to GRE water bridges is most likely due to the asymme-

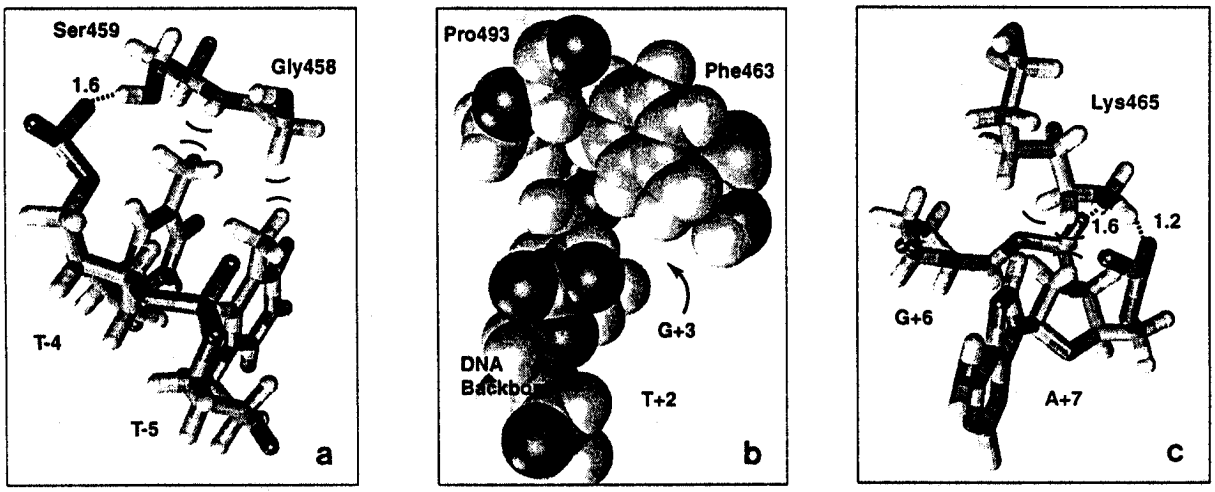

Fig. 13. Snapshots of three protein–DNA contacts observed during the simulations: (a) Gly-458 and Ser-459 contact methyls of T−4 and T−5 through van der Waals (vdW) interaction (brackets); Ser459-OH hydrogen bonds with phosphate of T−4 (dotted line, 1.6 Å); (b) Pro-493 and Phe-463 contact DNA backbone between phosphates G+3, T+2 through vdW interaction (brackets); (c) Lys-465 hydrogen bonds with phosphates at A+7, G+6 (dotted lines, 1.2 Å, 1.6 Å); vdW contact between Lys-465-Hε and A+7-H5′, H5″, H8′ (brackets).

try of this region of the protein, as noted already for His-472, Asp-473, and Tyr-474.

PROTEIN–PROTEIN CONTACTS

Protein–protein contacts serve in the recognition of the response element as shown by cooperativity experiments.[11,14,47] These contacts can be discerned from the contact matrices in Figure 14. The symmetry about the diagonal of each matrix indicates the symmetric nature of the interactions between P4-2 and P4-1 and between P3-2 and P3-1. Four symmetric dimer contacts, indicated by circles in Figure 14, have been identified in the crystallographic analysis: Asn-491 to Asn-491, Ile-487 to Leu-475, Ile-483 to Ala-477, and Asp-481 to Arg-479. The simulations of pgre3 and pgre4 preserve only the contacts between 1-Asn-491 and 2-Asn-491; this is surprising since the interactions between Arg-479 and Asp-481 are energetically most favorable according to our simulations.

Water bridges, which contribute to the dimer interactions, are listed in Table VI. The simulations of pgre4 and pgre3 exhibit significant differences among these water bridges, which are most likely due to differences in protein–DNA interactions for the two systems.

Arginine-479 to Asparagine-481

Salt bridges between Arg-479-NH_2 and Asp-481-OD, as described in the crystallographic analysis,[24] are conserved to varying degrees in pgre3, as listed in Table VII. These salt bridges constitute the overwhelming majority of the total protein–protein interaction energy contributing as much as −80 kcal/mol for a single amino acid. For P4-1-Asp-481 and P4-2-Arg-479, the salt bridge has shifted, relative to the crystallographic structure,[24] to an interaction between P4-1-Asp-481-O and P4-2-Arg-479-NH as listed in Table VII. The shift is due to the influence of water bridges between P4-1-Asp-481 and P4-2-Arg-479. Water bridges between P4-1-Arg-479 and P4-2-Asp-481 replace the salt bridge of the crystallographic structure.[24] Disruption of these extremely favorable interactions in pgre4 is characteristic of a lack of dimerization and recognition.

Isoleucine-483 to Alanine-477

The hydrogen bond between P4-2-Ile-483-NH and P4-1-Ala-477-O, as described in the crystallographic analysis,[24] is the only such hydrogen bond to remain intact throughout our simulations (table VII). The hydrogen bond between P4-1-Ile-483 and P4-2-Ala-477 is broken and the corresponding hydrogen bonds in pgre3 are substantially less frequent, yet van der Waals contacts between these residues are maintained, as evidenced by the contact matrix in Figure 14. Water bridges between P3-1-Gly-478 and P3-2-Ile-483, between P3-1-Arg-481 and P3-2-Ala-477, and between P3-1-Asn-491 and P3-2-Ala-477 have replaced the corresponding interactions between Ile-483 and Ala-477 in pgre3, as listed in Table VI. The decreased stability of these interactions in pgre3 implies that this hydrogen bond may not be favored as part of complete recognition.

Isoleucine-487 to Leucine-475

The dimer contacts, present in the crystallographic structure,[24] between the methyl groups of Ile-487 and Leu-475, are broken between P4-1-Leu-475 and P4-2-Ile-487 and between P3-1-Ile-487 and

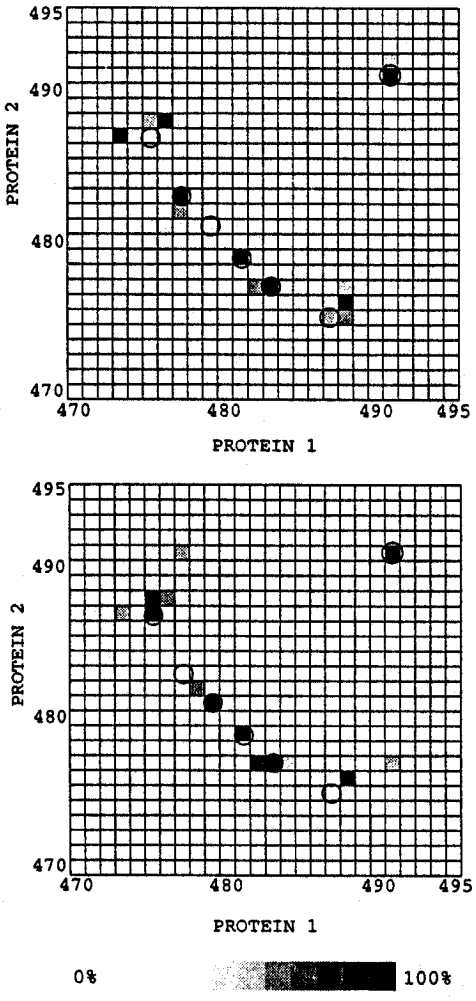

Fig. 14. Contact matrices for interprotein interactions (monomer 1, columns; monomer 2, rows) observed in pgre4 (top) and pgre3 (bottom); gray scale indicates frequency of contact; circles indicate contacts reported in the crystallographic anlaysis.[24]

P3-2-Leu-475 during the respective simulations; however, the contacts between P4-1-Ile-487 and P4-2-Leu-475 and between P3-1-Leu-475 and P3-2-Ile-487 remain intact to various degrees. The latter two contacts appear as one leg of an "L" in the contact matrices of Figure 14, while P4-2-Arg-488 forms a "line" of contacts, described below.

Arginine-488 to Leucine-475, Cysteine-476, Alanine-477

The "line" of dimer contacts, as observed for P4-2-Arg-488 is between Arg-488 from one monomer and Leu-475, Cys-476, and Ala-477 of the other monomer. This "line" of contacts is dominated by one amine of Arg-488 forming a strong hydrogen bond with the carbonyl of Cys-476. Weaker van der Waals contacts between Arg-488-Hβ and Ala-477-CH_3 and between Arg-488-Hδ and Leu-475-Hβ flank this hydrogen bond as indicated by the contact matrices in Figure 14. The most favorable conformation of Arg-488 achieves an interaction energy with the cognate monomer of approximately −20 kcal/mol. This conformation, as shown in Figure 15, is present to various degrees at all possible sites. For P3-2-Arg-488 a set of dimer contacts resembling an "L" in Figure 14 is formed due to the presence of a water bridge between P3-1-Cys-476-O and P3-2-Arg-488, listed in Table VI. The water bridge prevents the "line" from forming while allowing van der Waals contacts between P3-1-Leu-475 and P3-2-Ile-487, as described above, to remain.

Either the "line" or the "L" configuration connects an element of the second α-helix, amino acids 486–491, to an amino acid on the other monomer near the N-terminus of the dimer interface, thus, preserving the distribution of contacts among secondary structures. As stated above, the conformation and dynamics of the dimer loop have implications for the dynamics of the reading helix and, therefore, influences recognition of the DNA sequence.

Asparagine-491 to Asparagine-491

The hydrogen bond between P4-2-Asn-491-NH and P4-1-Asn-491-O is as described in the crystallographic analysis,[24] but the symmetric interaction between P4-2-Asn-491-O and P4-1-Asn-491-NH did not remain intact in our simulations. Each Asn-491 achieves a total interaction with the other monomer of approximately −20 kcal/mol in pgre4. In pgre3 the corresponding contacts represent the most frequent set of dimer contacts, but no hydrogen bonds are formed. P3-1-Asn-491 achieves an interaction with monomer 2 of approximately −5 kcal/mol and P3-2-Asn-491 achieves an interaction with monomer 1 of approximately −10 kcal/mol. Symmetric water bridges, listed in Table VI, between Asn-491-OD1 and Asn-491-O, have replaced the corresponding hydrogen bond in pgre3 and competition for a water bridge from P3-1-Asn-491 to P3-1-Ala-477 explains the lower protein–protein energy for P3-1-Asn-491.

The structural role of contacts between P3-1-Asn-491 and P3-2-Asn-491 is to connect the carboxy end of the second α-helix of P3-1, amino acids 486–491, to the carboxy end of the second α-helix of P3-2 forming, thus, an interprotein helix–helix interaction. The stability of this extended helix is also influenced by water bridges involving 1-Asp-473 and by salt bridges between each Lys-486 and DNA, described above.

DISCUSSION

Analysis of our simulations demonstrates that a modification of the crystallographic structure by means of molecular modeling, namely, restoration to the consensus DNA sequence and removal of crystal packing contraints improves recognition. We have demonstrated that the glucocorticoid receptor, upon

TABLE VI. Water Bridges Contributing to Protein–Protein Interactions for pgre4 and pgre3

Monomer 1	Monomer 2	Occupancy (%)
	Water bridges for pgre3	
Asp-473 ND2-HD22	Lys-490 NZ-HZ2	44.1
Cys-476 O	Arg-488 NH1-HH12	47.0
Gly-478 N-HN	Ile-483 O	34.8
Arg-481 N-HN	Ala-477 O	34.9
Lys-490 O	Lys-490 NZ-HZ2	42.7
Lys-490 O	Lys-490 O	46.8
Asn-491 OD1	Ala-477 N-HN	35.6
Asn-491 O	Asn-491 OD1	40.2
Asn-491 OD1	Asn-491 O	48.3
	Water bridges for pgre4	
Asp-473 OD1	Ile-487 O	46.5
Asp-473 O	Asn-491 ND2-HD21	62.1
Arg-479 NH1-HH11	Arg-481 OD2	33.0
Arg-479 NH1-HH12	Arg-481 OD2	46.2
Asp-481 OD1	Arg-479 NH2-HH21	69.5
Asp-481 OD1	Arg-479 NH1-HH11	81.6

TABLE VII. Hydrogen Bonds Contributing to Protein–Protein Interactions for pgre4 and pgre3

Monomer 1	Monomer 2	Occupancy (%)
	Hydrogen bonds for pgre3	
Asn-473 ND2-HD21	Ile-487 O	44
Arg-479 NH1-HH11	Asp-481 OD2	97
Arg-479 NH2-HH22	Asp-481 O	62
Arg-479 NH2-HH22	Asp-481 OD2	68
Ile-483 N-HN	Ala-477 O	47
Arg-488 NH2-HH21	Cys-476 O	100
Asp-481 OD1	Arg-479 NH1-HH11	45
Asp-481 OD2	Arg-479 NH1-HH11	77
Asp-481 OD2	Arg-479 NH2-HH21	45
	Hydrogen bonds for pgre4	
Asn-473 ND2-HD21	Ile-487 O	87
Arg-488 NH2-HH21	Cys-476 O	100
Asp-481 O	Arg-479 NH2-HH21	76
Ala-477 O	Ile-483 N-HN	99
Cys-476 O	Arg-488 NH2-HH22	97
Asn-491 O	Asn-491 ND2-HD22	68

association with its cognate DNA, alters the conformation of the DNA strand. The simulations also explain the observed significance of several amino acids of the GR DNA binding domain.

The analysis of protein–DNA and protein–protein interaction energies and contacts demonstrates that our manipulations of the crystallographic structure were successful in achieving a more favorable protein–DNA complex, i.e., better recognition, and more favorable protein–protein dimer interactions. The removal of crystallographic packing constraints and Hoogsteen-like interactions,[50] which in the crystal form join the ends of the DNA strands across the boundaries of crystal units,[24] allowed the systems to relax toward an energetically more favorable conformation. The resulting protein–DNA interactions appear to be symmetric for P3-2 and P3-1, with the exception of the contacts to DNA made by His-472, Asp-473, and Tyr-474, residues affected by these amino acids and Lys-490. The protein–protein interactions are relatively symmetric with the exception of interactions involving Ala-477 and, to a lesser extent, Arg-488. Water bridges have been identified that are related to these asymmetries. Sufficient sampling of conformational space was not achieved during the time scale of the present molecular dynamics simulations to determine if the remaining asymmetric interactions are due to insufficient relaxation or if asymmetry is inherent. Greater symmetry was achieved for these interac-

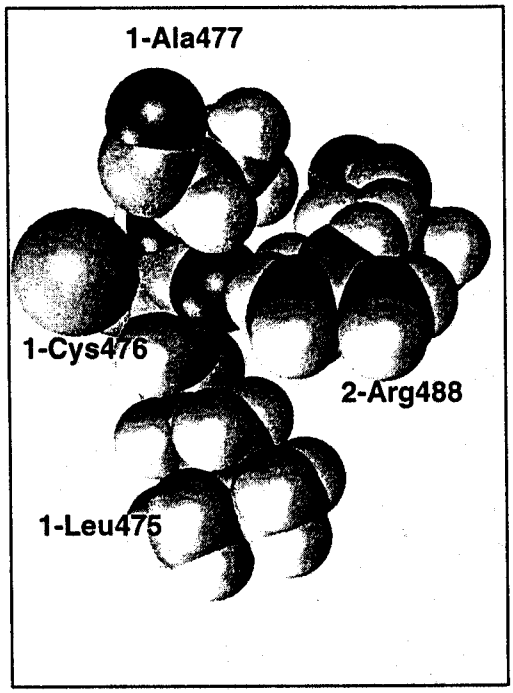

Fig. 15. Dimer contacts between Arg-488 and Leu-475, Cys-476, and Ala-477. Arg-488-NH_2 hydrogen bonds stongly with Cys-476-O. Weaker van der Waals contacts between Arg-488-Hβ and Ala-477-CH_3 and between Leu-475-Hβ and Arg-488-Hδ are also shown.

tions in simulations by Harris et al.[28] based on a model structure.

Our simulations identified protein–DNA interactions, particularly, the interactions involving Gly-458, Ser-459, Phe-463, and Lys-465, which correspond to elements that have proven to be significant in the ability of nuclear hormone receptors to recognize specific response elements.[8–10,51] These contacts were possible only due to a closer contact between the protein and the DNA, i.e., were not observed for the crystallographic structure[24] nor in other simulations.[27,28] The latter discrepancy is consistent with the fact that the closer contact between the protein and the DNA that we observe is the result of greater deformations of the DNA than were reported by Harris et al.[28] or Eriksson et al.[27]

Comparison of our simulation of gre to our simulations of pgre4 and pgre3 demonstrates that the glucocorticoid receptor induces significant conformational changes in the target DNA. GR-DBD dimers induce writhe in the DNA, which is manifest as a local bend away from the protein and as a displacement of the axis of the GRE. This is not observed for the simulation of gre, which contained only a DNA segment. Our measure of the degree of bending is in agreement with observations for homologous systems[20,21] and is qualitatively the same for GRE3 and GRE4. The displacement of the DNA axis, as it passes through the region of contact with the protein, has not been previously reported for this class of proteins, and, to date, no experimental studies of DNA bending induced by the GR-DBD dimer have been reported. The DNA is also found to unwind as a result of the protein–DNA interactions. Our simulations demonstrate that the rate and degree of unwinding is sequence-dependent, indicating that DNA unwinding is part of the recognition mechanism.

The simulations by Harris et al.[28] and by Eriksson et al.[27] employed counterions for charge neutralization and cut-off of electrostatic forces. Counterions and cut-off reduce the influence of the protein on the DNA, in particular, underestimating the influence of highly energetic salt bridges between the protein and the DNA phosphate groups, for example, the interactions we report between Lys-486 and the DNA. Thus, the protein–DNA interactions in the respective simulations may not have sufficient strength to deform the DNA to the extent observed experimentally.[20,21]

The writhed conformation and unwinding of the DNA induced by the GR-DBD have implications for the regulatory function of the receptor. Viewed in the context of DNA topology, the linking number, writhe, and twist form a conserved quantity.[52] Thus, local changes of these quantities influence the overall topology of circular DNA and the topological equivalent of circles. The latter includes segments of DNA constrained at two points, such as linker DNA between histones, so the protein may achieve its regulatory function by altering the nucleosomal packing.[53] Viewed in the context of transcription machinery, the writhe, which introduces a bend and a displacement of the DNA helical axis in this case, can directly affect the binding of the DNA to the histone octomer, so the protein may achieve its regulatory function by directly altering the nucleosome complex.

ACKNOWLEDGMENTS

We would like to thank Paul Sigler and co-workers for making the crystal structure of the GR-DBD/DNA complex available to us, Helmut Heller for extensive instructions on the use of EGO, and Parsytec Computers for technical assistance with the GCel-64 transputer. We would like to thank Bill Humphrey and Andrew Dalke for adapting the visualization package vmd,[54] which allowed us to generate many of the graphic images presented in this article. Finally we would like to thank Ann Nardulli, Dave Shapiro, and their co-workers for assistance and for an introduction to nuclear hormone receptor proteins. This work was supported by grants from the National Institutes of Health (PHS 5 P41 RR05969-04), the National Science Foundation (BIR-9318159 and ASC-8902829), and the Roy J. Carver Charitable Trust.

REFERENCES

1. Laudet, V., Hänni, C., Coll, J., Catzeflis, F., Stéhelin, D. Evolution of the nuclear receptor gene superfamily. EMBO J. 11(3):1003–1013, 1992.
2. Martinez, E., Givel, F., Wahli, W. A common ancestor DNA motif for invertebrate and vertebrate hormone response elements. EMBO J. 10:263–268, 1991.
3. Evans, R. M. The steroid and thyroid hormone receptor superfamily. Science 240:889–895, 1988.
4. Freedman, L. P., Luisi, B. F., Korszun, Z. R., Basavappa, R., Sigler, P. B., Yamamoto, K. R. The function and structure of the metal coordination sites within the glucocorticoid receptor DNA binding domain. Nature (London) 334: 543–546, 1988.
5. Harrison, S. C. A structural taxonomy of DNA-binding domains. Nature (London) 353:715–719, 1991.
6. Chin, W. W. Nuclear thyroid hormone receptors. In: "Nuclear Hormone Receptors." Parker, M. G. (ed.). New York: Academic Press, 1991:79–102.
7. Martinez, E., Wahli, W. Characterization of hormone response elements. In: "Nuclear Hormone Receptors." Parker, M. G. (ed.). San Diego, CA: Academic Press, 1991: 125–154.
8. Danielsen, M., Hinck, L., Ringold, G. M. Two amino acids within the knuckle of the first zinc finger specify DNA response element activation by the glucocorticoid receptor. Cell 57:1131–1138, 1989.
9. Mader, S., Kumar, V., Verneuil, H. d., Chambon, P. Three amino acids of the oestrogen receptor are essential to its ability to distinguish an oestrogen from a glucocorticoid-responsive element. Nature (London) 338:271–274, 1989.
10. Umesono, K., Evans, R. M. Determinants of target gene specificity for steroid/thyroid hormone receptors. Cell 57: 1139–1146, 1989.
11. Eriksson, P., Wrange, O. Protein-protein contacts in the glucocorticoid receptor homodimer influence its DNA binding properties. J. Biol. Chem. 265:3535–3542, 1990.
12. Härd, T., Dahlman, K., Duke, J. C., Gustafsson, J., Rigler, R. Cooperativity and specificity in the interactions between DNA and the glucocorticoid receptor DNA-binding domain. Biochemistry 29:5358–5364, 1990.
13. Dahlman-Wright, K., Siltala-Roos, H., Carlstedt-Duke, J., Gustafsson, J. Protein-protein interactions facilitate DNA binding by the glucocorticoid receptor DNA-binding domain. J. Biol. Chem. 265:14030–14035, 1990.
14. Tsai, S. Y., Tsai, M., O'Malley, B. W. Cooperative binding of steroid hormone receptors contributes to transcriptional synergism at target enhancer elements. Cell 57:443–448, 1989.
15. Härd, T., Kellenbach, E., Boelens, R., Maler, B. A., Dahlman, K., Freedman, L. P., Carlstedt-Duke, J., Yamamoto, K. R., Gustafsson, J., Kaptein, R. Solution structure of the glucocorticoid receptor DNA-binding domain. Science 249: 157–160, 1990.
16. Schwabe, J. W. R., Neuhaus, D., Rhodes, D. Solution structure of the DNA-binding domain of the oestrogen receptor. Nature (London) 348:458–461, 1990.
17. Vliet, P. C. v. d., Verrijzer, C. P. Bending of DNA by transcription factors. BioEssays 15(1):25–32, 1993.
18. Crothers, D. M., Wu, H. M. The locus of sequence-directed and protein-induced DNA bending. Nature (London) 308: 509–513, 1984.
19. Thompson, J. F., Landy, A. Empirical estimate of protein-induced DNA bending angles: applications to lambda site-specific recombinaton complexes. Nucleic Acids Res. 16: 9687–9705, 1988.
20. Nardulli, A. M., Shapiro, D. J. Binding of the estrogen receptor DNA-binding domain to the estrogen response element induces DNA bending. Mol. Cell. Biol. 12:2037–2042, 1992.
21. Sabbah, M., Ricousse, S. L., Redeuith, G., Baulieu, E. Estrogen receptor-induced bending of the xenopus vitellogenin A_2 gene hormone response element. Biochem. Biophys. Res. Commun. 185(3):944–952, 1992.
22. Wolffe, A. P. Nucleosome positioning and modification: Chromatin structure that potentiate transcription. Trends Biochem. Sci. 19(6):240–244, 1994.
23. Schwabe, J. W. R., Chapman, L., Finch, J. T., Rhodes, D. The crystal structure of the estrogen receptor DNA-binding domain bound to DNA: How receptors discriminate between their response elements. Cell 75(5):567–578, 1993.
24. Luisi, B. F., Xu, W. X., Otwinowski, Z., Freedman, L. P., Yamamoto, K. R., Sigler, P. B. Crystallographic analysis of the interaction for the glucocorticoid receptor with DNA. Nature (London) 352:497–505, 1991.
25. Bishop, T., Schulten, K. Molecular dynamics study of a sequence specific protein-DNA interaction. In: "Computational Approaches in Supramolecular Chemistry." Wipff, G. (ed.). Boston: Kluwer Academic Publishers, 1994:419–439.
26. Eriksson, M., Härd, T., Nilsson, L. Molecular dynamics simulation of a DNA binding protein free and in complex with DNA. In: "Computational Approaches in Supramolecular Chemistry." Wipff, G. (ed.). Boston: Kluwer Academic Publishers, 1994:457–475.
27. Eriksson, M., Härd, T., Nilsson, L. Molecular dynamics simulations of the glucocorticoid receptor DNA-binding domain in complex with DNA and free in solution. Biophys. J. 68:402–426, 1995.
28. Harris, L. F., Sullivan, M. R., Popken-Harris, P. D., Hickok, D. F. Molecular dynamics simulations in solvent of the glucocorticoid receptor protein in complex with a glucocorticoid response element dna sequence. J. Biom. Struct. Dyn. 12(2):249–270, 1994.
29. Brünger, A. T. X-plor, version 3.1, a system for X-ray crystallography and NMR. The Howard Hughes Medical Institute and Department of Molecular Biophysics and Biochemistry, Yale University, 1992.
30. Kitzing, E. v. Modeling DNA structure: Molecular mechanics and molecular dynamics. Methods Enzymol. 211: 449–467, 1992.
31. Jayaram, B., Aneja, N., Rajasekaran, E., Arora, V., Das, A., Ranganathan, V., Gupta, V. Modelling DNA in aqueous solutions. J. Sci. Indust. Res. 53:88–105, 1994.
32. Lamm, G., Wong, L., Pack, G. R. Monte carlo and poisson-Boltzmann calculations of the fraction of counterions bound to DNA. Biopolymers 34:227–237, 1994.
33. Beveridge, D. L., Ravishanker, G. Molecular dynamics studies of DNA. Curr. Opinion Struct. Biol. 4:246–255, 1994.
34. Walberer, B., Schulten, K. WATER—A program for the implicit inclusion of water in molecular dynamics simulations of proteins. Beckman Institute Technical Report TB-91-17, University of Illinois, 1991.
35. Jorgensen, W. L., Chandrasekhar, J., Madura, J. D., Impey, R. W., Klein, M. L. Comparision of simple potential functions for simulating liquid water. J. Chem. Phys. 79: 926–935, 1983.
36. Heller, H., Grubmüller, H., Schulten, K. Molecular dynamics simulation on a parallel computer. Mol. Simulation 5:133–165, 1990.
37. Banko, B., Heller, H. User manual for EGO—Release 1.1. Beckman Institute Technical Report TB-92-07, University of Illinois, 1991.
38. Bishop, T., Heller, H., Schulten, K. Molecular dynamics on parallel computers: Applications for theoretical biophysics. In: "Toward Teraflop Computing and New Grand Challenge Applications." Kalia, R. K., Vashishta, P. (eds.). New York: Nova Science Publishers, 1995:129–138.
39. Brooks, B. R., Bruccoleri, R. E., Olafson, B. D., States, D. J., Swaminathan, S., Karplus, M. CHARMm: A program for macromolecular energy, minimization, and dynamics calculations. J. Comp. Chem. 4(2):187–217, 1983.
40. Grubmüller, H., Heller, H., Windemuth, A., Schulten, K. Generalized Verlet algorithm for efficient molecular dynamics simulations with long-range interactions. Mol. Simulation 6:121–142, 1991.
41. Streett, W. B., Tildesley, D. J., Saville, G. Multiple time-step methods in molecular dynamics. Mol. Phys. 35(3): 639–648, 1978.
42. Allen, M. P., Tildesley, D. J. "Computer Simulation of Liquids." New York: Oxford University Press, 1987.
43. Ryckaert, J.-P., Ciccotti, G., Berendsen, H. J. C. Numerical integration of the Cartesian equations of motion of a system with constraints: Molecular dynamics of *n*-alkanes. J. Comp. Phys. 23:327–341, 1977.
44. Sklenar, H., Etchebest, C., Lavery, R. The definition of generalized helicoidal parameters and of axis of curvature for irregular nucleic acids. Proteins 6:46–60, 1989.

45. Ravishanker, G., Swaminathan, S., Beveridge, D. L., Lavery, R., Sklenar, H. Conformational and helicoidal analysis of 30 ps of molecular dynamics on the d(CGCGAATTCGCG) double helix. J. Biomol. Str. Dyn. 6:669, 1989.
46. Saenger, W. (ed.). "Principles of Nucleic Acid Structure." New York: Springer-Verlag, 1984.
47. Wright, A. P. H., Gustafsson, J. Mechanism of synergistic transcriptional transactivation by the human glucocorticoid receptor. Proc. Natl. Acad. Sci. U.S.A. 88:8283–8287, 1991.
48. Dover, S. D. Symmetry and packing in B-DNA. J. Mol. Biol. 110:699–700, 1977.
49. Klug, A., Rhodes, D. Helical periodicity of DNA determined by enzyme digestion. Nature (London) 286:573–578, 1980.
50. Hoogsteen, K. The crystal and molecular structure of a hydrogen-bonded complex between 1-methyl thymin and 9-methyl adenine. Acta Crystallogr. 16:907–916, 1963.
51. Parker, M. G. (ed.). "Nuclear Hormone Receptors." San Diego, CA: Academic Press, 1991.
52. White, J. H. Self-linking and the gauss integral in higher dimensions. Am. J. Math. 91:693–728, 1969.
53. Cozzarelli, N. R., Wang, J. C. (eds.). "DNA Topology and Its Biological Effects." Cold Spring Harbor, NY: Cold Spring Harbor Laboratory Press, 1990.
54. Humphrey, W., Dalke, A., Schulten, K. VMD—visual molecular dynamics. Submitted.
55. Sinha, A. B., Schulten, K., Heller, H. Performance analysis of a parallel molecular dynamics program. Comput. Phys. Commun. 78:265–278, 1994.
56. Danielsen, M. Structure and function of the glucocorticoid receptor. In: "Nuclear Hormone Receptors." Parker, M. G. (ed.). San Diego, CA. Academic Press, 1991:39–78.
57. Kraulis, P. MOLSCRIPT—a program to produce both detailed and schematic plots of protein structures. J. Appl. Crystallogr. 24:946–950, 1991.